Volume 3
Number 11
November 2024
Pages 1761–1878

Sensors & Diagnostics

rsc.li/sensors

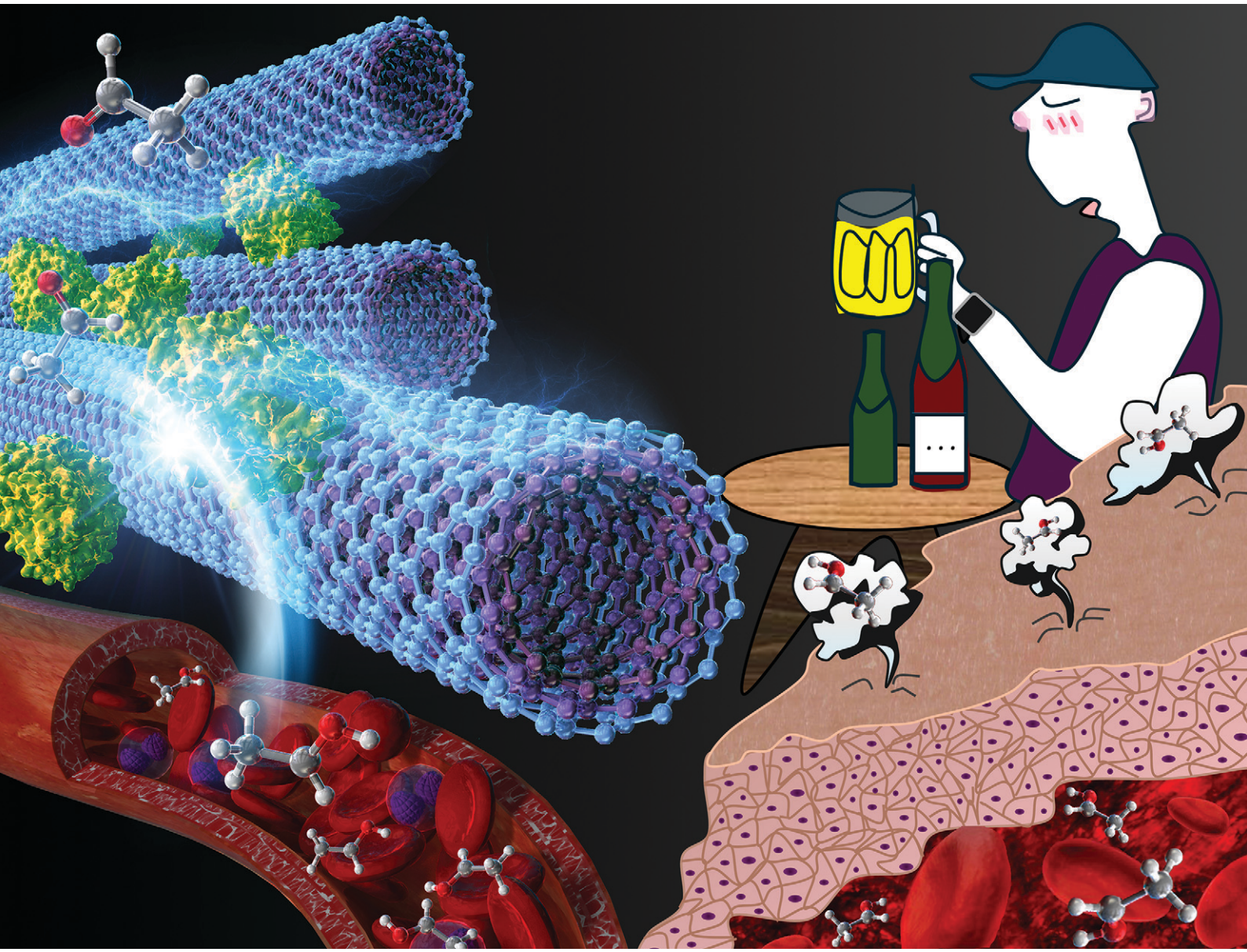

ISSN 2635-0998

ROYAL SOCIETY OF CHEMISTRY

PAPER

Masato Tominaga *et al.*

Highly sensitive flux-type non-invasive alcohol biosensor based on direct electron transfer of PQQ-dependent alcohol dehydrogenases adsorbed on carbon nanotubes

Sensors & Diagnostics

PAPER

View Article Online
View Journal | View Issue

Cite this: *Sens. Diagn.*, 2024, **3**, 1827

Highly sensitive flux-type non-invasive alcohol biosensor based on direct electron transfer of PQQ-dependent alcohol dehydrogenases adsorbed on carbon nanotubes†

Citra Dewi Rakhmania, [a] Yoshi Izzuddin Azhar,[b] Kenji Shida,[c] Erika Shinchi,[d] Taiki Adachi,[e] Keisei Sowa, [e] Yuki Kitazumi,[e] Osamu Shirai [e] and Masato Tominaga *[ab]

Received 16th May 2024,
Accepted 21st September 2024

DOI: 10.1039/d4sd00161c

rsc.li/sensors

Ethanol gas excreted by human skin can be used to determine auto-brewery syndrome (drunken disease), blood alcohol levels, and/or a body state of alcoholism. Considering the limitations of continuous non-invasive alcohol gas monitoring based on the electrochemical method, which requires high sensitivity and selectivity, a CNF film sensor was developed. This sensor was developed by utilizing pyrroloquinoline quinone-dependent alcohol dehydrogenase (PQQ-ADH) and multiwalled carbon nanotubes (MWCNTs) based on cellulose nanofiber (CNF) film platform. With a compact design, a PQQ-ADH/MWCNTs/CNF film sensor was built in a three-electrode system. This system could continuously detect ethanol gas with ultra-high sensitivity, a wide detection range (24 ppb–25 ppm), and high selectivity for ethanol. Finally, the CNF film sensor was used for ethanol gas monitoring in the human subject, and we were able to detect metabolism abnormalities of the subject by analyzing the declining slope (detoxification rate) of the ethanol gas concentration monitored. The CNF film sensor aims to gain valuable insights and enhance future standard health screening practices through non-invasive wearable daily monitoring sensors.

Introduction

Nowadays, biosensors are well recognized in various disciplines, particularly biomedical, because of their remarkable sensitivity and selectivity.[1–3] Biosensors provide the crucial ability to continuously measure the concentration of metabolites in biological samples.[4] This makes biosensors a beneficial choice for wearable healthcare monitoring systems. Moreover, non-invasive methods have been investigated as future alternatives for health monitoring.[5,6] This type of system enables subjects to be monitored anytime to guarantee proper diagnosis and treatment without causing inconvenience or reducing the user's comfort. Several non-invasive monitoring techniques have been reported, including the use of tears, fluid, saliva, sweat, breath, and skin gas.[5–9] Skin gas is a metabolic product containing mixed volatile organic compounds (VOCs) at extremely low concentrations (ppb levels).[5,8–11] Specific compounds in skin gas are closely related to human health conditions.[8–11] Further, skin gas is easier to monitor continuously in real-time by using wearable sensors as compared to the breath sensors.[8,12] Wearable skin gas sensors require reaction selectivity, flexibility, stretchability, and safety.

Ethanol gas is often present in the human body. Ethanol gas is used to determine auto-brewery syndrome (drunken disease), blood alcohol level, and/or a body state of alcoholism.[9,13,14] Alcohol consumption correlated with public health concerns worldwide, and many alcohol-related abuse cases have resulted in various crimes,[15] including traffic crimes.[15,16] A licensed driver is categorized as driving under the influence (DUI) of alcohol under legal regulations if the blood alcohol concentration (BAC) is higher than 0.03% (or 0.15 ppm breath alcohol concentration) in Japan,[17] 0.5% in Europe,[18] 0.15% in the USA,[19] and 0.05% in Australia.[20] Further, monitoring alcohol levels provides important evidence in forensic and legal medicine.[16]

[a] *Graduate School of Science and Engineering, Saga University, 1 Honjomachi, Saga 840-8502, Japan. E-mail: masato@cc.saga-u.ac.jp*
[b] *Department of Chemistry and Applied Chemistry, Saga University, 1 Honjomachi, Saga 840-8502, Japan*
[c] *Faculty of Engineering, Kumamoto University, Kumamoto 860-8555, Japan*
[d] *Analytical Research Center for Experimental Science, Saga University, 1 Honjomachi, Saga 840-8502, Japan*
[e] *Divison of Applied Life Sciences, Graduate School of Agriculture, Kyoto University, Sakyo, Kyoto 606-8502, Japan*

† Electronic supplementary information (ESI) available. See DOI: https://doi.org/10.1039/d4sd00161c

The most common detection methods are based on electrochemical (amperometry),[21] fluorescence,[22–24] chemiluminescence,[25] optical,[25] and electrical resistance change.[26,27] However, only fluorometry-based sensors have been developed specifically for monitoring non-invasive alcohol gas.[22–24] Several commercialized electrochemical-based sensors were limited for transdermal alcohol detection.[21,28] Furthermore, the development of continuous non-invasive alcohol gas sensors is limited by the extremely high requirements for sensitivity, specificity, and resistance to humidity.

In this study, we achieved ultra-high sensitivity and specific ethanol detection based on the electrochemical method by utilizing an enzyme-based reaction on a modified multiwalled carbon nanotubes (MWCNTs)/cellulose nanofiber (CNF) film (CNF film sensor). CNF is used due to its good attachment for conductive materials and its eco-friendly characteristics.[29] We fabricated a three-electrode system by modifying a pyrroloquinoline quinone-dependent alcohol dehydrogenase (PQQ-ADH) on the MWCNTs on CNF film as the working electrode. PQQ-ADH was chosen because it did not require a mediator (able to transfer electrons directly) and was considered an attractive enzyme for compact biosensor development.[30,31] MWCNTs are proven to have a large surface area, high electrical conductivity, and also good immobilization substrate for the enzymes.[32–34] By utilizing the direct electron transfer-type bioelectrocatalysis of PQQ-ADH, the CNF film sensor was designed to be a highly sensitive compact sensor for non-invasive alcohol gas detection. The CNF film sensor was optimized and characterized to ensure high direct electron efficiency. Finally, the performance of the CNF film sensor was verified by ethanol gas monitoring in human subjects.

Experimental

Materials

Nanoforest-S BB made from bamboo using an aqueous counter-collision (ACC) method was used as the CNF and was obtained from Chuetsu Pulp and Paper Co., Ltd. (Tokyo, Japan).[35,36] MWCNTs (purity: ±98%, length: 3–6 μm, outer diameter: 10 nm ± 1 nm, inner diameter: 4.5 nm ± 0.5 nm) were obtained from Sigma Aldrich (St. Louis, MO, USA) and were used as received. *N*,*N*-Dimethylacetamide (DMAc) and fine powder of polybenzimidazole (PBI) were purchased from FUJIFILM Wako Pure Chemical Industries (Osaka, Japan) and Sato Light Industrial Co., Ltd. (Tokyo, Japan), respectively. A glassy carbon electrode (GCE, 3 mm in diameter) was purchased from BAS Inc. (Tokyo, Japan). Ethanol (99.5%), 1-propanol (99.5%), 2-propanol, acetone (99.5%), and methanol (99.8%) were purchased from FUJIFILM Wako Pure Chemical Industries. Acetate buffer solutions were prepared by mixing CH_3COONa (FUJIFILM Wako Pure Chemical) and CH_3COOH (FUJIFILM Wako Pure Chemical). The solution pH was adjusted to pH 5.5 with 0.1 M HCl and 0.1 M NaOH. Further, 2 mM $CaCl_2$ (FUJIFILM Wako Pure Chemical) was added to the buffer solution as a PQQ-ADH stabilizer.[30] All other reagents were of analytical grade and were used as received. All solutions were prepared with deionized water (resistivity > 18.2 MΩ cm) obtained using a Milli-Q water purification system (Millipore, Billerica, MA, USA).

PQQ-ADH preparation

A pyrroloquinoline quinone-dependent alcohol dehydrogenase (PQQ-ADH) overexpression system was described previously,[30,31,37,38] where the plasmid (harboring a sequence-verified putative region with *adhAB* genes, [*adh-pro*], *adhS*, and *adhAB*) was introduced into native *Gluconobacter oxydans* NBRC12528. The expressed PQQ-ADH was extracted from mutated *G. oxydans* as previously reported using membrane fractionation,[39] where the extracted solution contained 0.1% Triton® X-100, 10% sucrose, and 2 mM calcium chloride ($CaCl_2$). The PQQ-ADH activity in 0.1 M acetate buffer at pH 5.5 was analyzed to be 343 U mg^{-1} by spectrophotometry based on ferricyanide reduction at 417 nm as described in the ESI† (Fig. S1–S7). Here, we assumed that 2 electrons will be produced and transferred by PQQ-ADH per ethanol molecule. Hence, one unit of the PQQ-ADH activity was described as the amount of enzyme needed to oxidize 1 μmol of ethanol per minute. Enzyme concentrations were estimated using the Pierce™ BCA Protein assay kit (Thermo Fisher Scientific, Inc, USA) with bovine serum albumin as the standard.

Preparation of PQQ-ADH modified GCE

The GCE was polished with a 0.05 μm alumina suspension on a polishing pad, rinsed with Milli-Q water, and sonicated in Milli-Q water for 3 minutes. Then, 100 μL of MWCNTs-dispersed solution was cast on the polished GCE surface and dried overnight under vacuum (±0.06 MPa). The MWCNTs-dispersed solution was prepared by utilizing an ultrasonic homogenizer for 15 minutes to disperse MWCNTs (8 mg) in water (10 mL). The MWCNTs/GCE were then modified by immersing the electrode surface into a PQQ-ADH enzyme solution (343 U mg^{-1}) at various adsorption times. The modified electrode was then gently rinsed with 0.1 M acetate buffer solution (pH 5.5 with 2 mM $CaCl_2$) to remove the excess PQQ-ADH. The electrochemical measurement was carried out in 0.1 M acetate buffer solution (pH 5.5 with 2 mM $CaCl_2$).

Preparation of CNF film sensor

A CNF film sensor was prepared, as shown (Fig. 1). First, a CNF film was prepared, as described in a previous study.[40] Briefly, 600 mg of 2.35 wt% CNF was dispersed in 20 mL of Milli-Q water using an ultrasonic homogenizer. Next, 10 mL of this CNF-dispersed solution was spread on a Teflon plate (4 × 10 cm) and heated at 140 °C on a hotplate until dried. The dried CNF films were cut to dimensions of 2 × 0.5 cm.

The MWCNTs- and PBI/MWCNTs-dispersed solutions were prepared as follows: the MWCNTs solution was prepared by dispersing MWCNTs (8 mg) in water (10 mL) using an

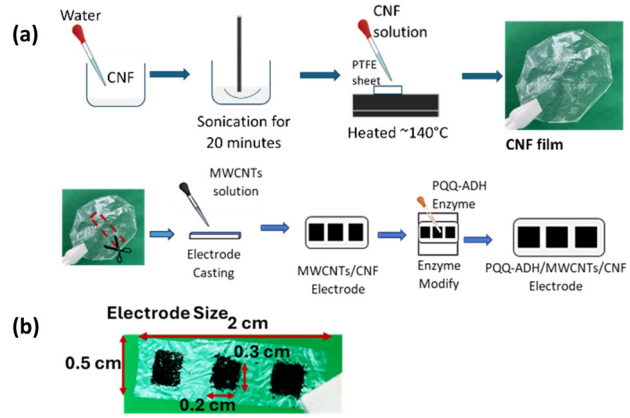

Fig. 1 Schematic illustration of (a) cellulose nanofiber (CNF) film sensor preparation, and (b) it's size.

ultrasonic homogenizer for 15 min. First, 40 mg of PBI was dissolved in 10 mL DMAc for 20 min using an ultrasonic homogenizer to prepare a PBI/DMAc solution. The PBI/MWCNTs solution was then prepared by dispersing MWCNTs (6 mg) and PBI/DMAc solution (60 μL) in DMAc (3 mL) using a sonicator for 135 min (15 min using a probe-type sonicator, followed by 2 h using a bath-type sonicator).

To prepare the MWCNTs/CNF sensor with the three-electrode system, the prepared CNF film surface (2 × 0.5 cm) was modified by drop casting with 10 μL of the MWCNTs solution for the working electrode, and 5 μL of the PBI/MWCNTs solution for each reference and counter electrode side. The prepared CNF film sensor was then heated and dried at 80 °C on a hotplate. The film electrode thickness was estimated to be 50 (± 5) μm.

The CNF film sensor surface was then treated with UV ozone for 1 min to remove organic contaminants from the MWCNTs surface. The working MWCNTs electrode surface was then modified by drop-coating with 7.5 μL of PQQ-ADH enzyme solution (343 U mg^{-1}) for 30 min. The electrode surface was then gently rinsed with 0.1 M acetate buffer solution (pH 5.5 with 2 mM $CaCl_2$) to remove excess PQQ-ADH. Before each electrochemical measurement, the CNF film sensor was immersed in 0.1 M acetate buffer solution (pH 5.5 with 2 mM $CaCl_2$) for 15 minutes to ensure the stability of the reference electrode (Fig. S20†). Additional *ca.* 100 μL acetate buffer solution was then dropped on the sensor surface prior to the electrochemical measurement (Fig. S18b†), to hydrate the electrodes as in previous studies.[41,42]

Ethanol gas detection and calibration curve

Ethanol gas produced using an evaporating system was collected in a 1 L Tedlar bag for each concentration of the evaporated ethanol solution (Fig. S8†). To construct a calibration curve, the collected gas was analyzed using gas chromatography (GC) and compared with standard ethanol gas produced using a gas permeator. The obtained calibration curve (Fig. S9†) was used to determine the ethanol gas concentration during the electrochemical measurements for the CNF film sensor.

Alcohol gas monitoring on human subject

The ethics committee of the Faculty of Medicine, Saga University, had approved the experiment of non-invasive alcohol gas monitoring, with approval number R5-36. The experiment was conducted in compliance with all guidelines and regulations of Saga University. The observation was carried out after informed consent was obtained from all subjects who remained alcohol—and drug-free for 72 hours before the experiment. The CNF film sensor was attached to the two healthy male subjects on the left volar wrist by using a band-aid. A plastic spacer with a rectangular hole of 3.5 mm × 16 mm was placed on the top of the subject skin to limit the observed skin surface. The band-aid was used to provide a secure attachment for the sensor cell. The band-aid (CL9LL) was obtained from Nichiban Co., Ltd (Japan). The skin gas amperometry baseline was then measured for *ca.* 16 min before drinking the alcohol.

Instrumentation

A probe-type BRAN-SON 5520 sonicator (Kanagawa, Japan) and/or bath-type AS ONE US-3A sonicator (Osaka, Japan) was used to disperse the solutions. A UV-ozone treatment system (model OCA-150L-D, Eye Graphics Co., Japan) was used to remove organic contaminants from the electrode surface.[43] Scanning electron microscopy (SEM) imaging was performed using a JSM-7600F microscope (JEOL, Japan). The sample surfaces were coated with osmium nanoparticles of approximately 5 nm diameter by sputtering before SEM analysis. Standard ethanol gas was produced using a gas permeator (PD-1B-2; Gastec Co., Kanagawa, Japan). Gas chromatography was performed using a GC-2014 Shimadzu (Kyoto, Japan) and employed an HP-5 column (part number 19091J-413 with inner diameter 0.32 mm and film thickness 0.25 μm). The pH was recorded using a pH meter (AUT-501; DKK-TOA Corp., Tokyo, Japan). Spectrophotometric measurements were performed using a UV-VIS 2600 spectrometer (Shimadzu, Kyoto, Japan). Quartz crystal microbalance (QCM) measurements were performed using a QCM2000 instrument (Initium Co., Japan). An Au film was deposited on an AT-cut quartz crystal with a fundamental resonance frequency of 27 MHz, and its surface was polished to a mirror-like finish. The roughness factor of a film of the QCM was estimated to be 1.02 (Ra = 5.2 nm).[44] All the electrochemical measurements were performed using an electrochemical analyzer (ALS/CHI 660A, ALS Co., Ltd, Tokyo, Japan). For the laboratory experiments, Ag|AgCl|saturated KCl (+199 mV *vs.* normal hydrogen electrode) and a platinum plate were used as the references and counter electrodes. For the human skin tests, CNF electrodes were used, and the reference was measured to be (+200 mV *vs.* Ag|AgCl|saturated

KCl) in nominal conditions. All potentials were reported with respect to Ag|AgCl|saturated KCl at 25 °C.

Results and discussion

PQQ-ADH adsorption behavior

Fig. 2(a) shows the cyclic voltammograms of the PQQ-ADH/MWCNTs modified GCE in 0.1 M acetate buffer solution (pH 5.5 with 2 mM $CaCl_2$) in the absence (broken line) and presence (solid line) of ethanol. The catalytic oxidation current was observed starting from −0.1 V (*vs.* Ag|AgCl| saturated KCl). The catalytic current was significantly higher than that of the GCE without the MWCNTs modification (Fig. S10 in ESI†). Further, the observed current density in our modified electrode was much higher than that reported in previous studies using bare Au,[45] Au–Pt,[46] GC,[46] single-walled carbon nanotube,[47] few-walled carbon nanotubes,[34] and MWCNTs[30,48] electrodes. The observed onset potential for the catalytic current in our results was similar to that in previous reports, indicating that the observed catalytic current was attributed to direct electron transfer (DET) between the adsorbed PQQ-ADH and the MWCNTs surface (illustrated in Fig. 2b) as explained previously.[30,31] Many positively charged amino acid residues are known to be present around the Heme 1C (Fig. 2b). This Heme 1C portion is expected to orient the PQQ-ADH molecules appropriately for DET through interaction with the MWCNTs surface.[31] The MWCNTs surface has a hydrophobic structure and negative charge. This negative charge is attributed to oxygen-containing functional groups such as –C═O, –COOH, and –C–OH because of sp^2 carbon defects. The Raman spectrum of MWCNTs showed a large D-band peak (Fig. S11†), indicating the expected oxygen-containing functional group in the MWCNTs.[49] These properties of MWCNTs suggest a suitable PQQ-ADH molecular orientation on the MWCNTs surface *via* electrostatic interactions between the Heme 1C portion and the MWCNTs surface.

The catalytic current was highly dependent on the enzyme modification time (Fig. 2a). The catalytic current increases with increasing PQQ-ADH adsorption time. Interestingly, the catalytic current spiked at 20–30 min (Fig. 2c). This behavior is considered abnormal because the catalytic current generally shows an increase as Langmuir isotherm adsorption.[44] QCM measurements were thus conducted to further analyze the adsorption behavior of PQQ-ADH. First, the electrochemical active surface area (ECSA) of MWCNTs was estimated to be 9.6 cm^2 (Fig. S12†). The ratio of ECSA to geometric electrode area (0.07 cm^2) is *ca.* 135. This value is similar to the other modified MWCNTs electrode in previous research.[51] The change in PQQ-ADH mass was estimated by QCM results (Fig. S13–S15†). Fig. 2(c) shows the surface concentration of adsorbed PQQ-ADH as a function of the modification time, where the surface area indicates the ECSA of MWCNTs. The amount of enzyme increased rapidly within a few seconds and then plateaued at approximately 30 min. The maximum amount of adsorbed PQQ-ADH was estimated to be *ca.* 9.2 pmol cm^{-2}. Based on the size of the PQQ-ADH molecule 70.4 × 117.4 Å (Fig. S16 and S17†), the theoretical maximum enzyme loading was expected to be *ca.* 2.4–6.7 pmol cm^{-2}, which was strongly dependent on the adsorption molecular orientation of the enzyme on the MWCNTs surface. From the QCM results and the value of the theoretically expected maximum enzyme loading, the maximum amount of PQQ-ADH surface concentration obtained was suggested to be monolayer adsorption.

The catalytic current was expected to increase with increasing PQQ-ADH surface concentration. The QCM results indicated that the adsorption behavior was similar to that of the Langmuir isotherm model. However, as mentioned above, the catalytic current behavior was remarkably different from the PQQ-ADH adsorption behavior during 20–30 min of modification time (Fig. 2c).

After comprehensively and carefully considering the catalytic current behavior, enzyme adsorption behavior, and its analysis, we came to the following conclusions, as shown in Fig. 3: where at lower PQQ-ADH surface concentration, the adsorbed PQQ-ADH molecular orientation is comparatively random (≤20 min adsorption time). Then, hydrophobic

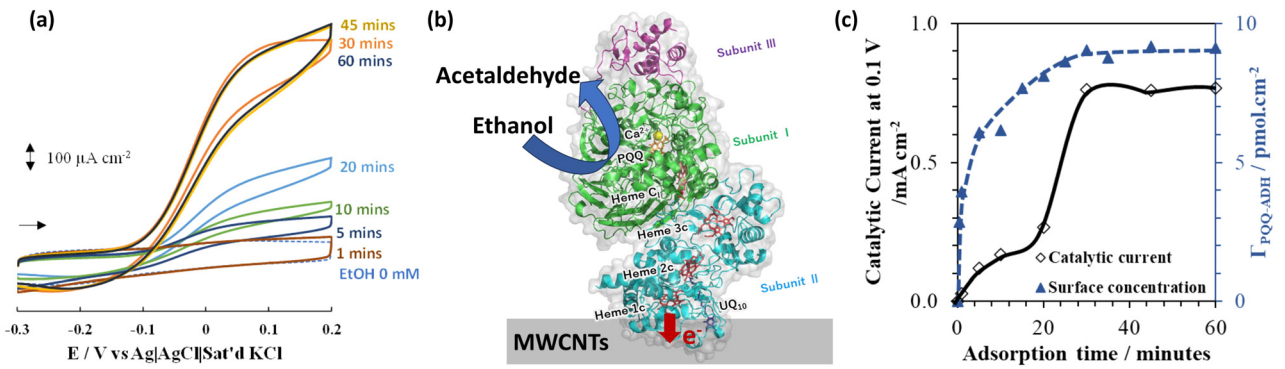

Fig. 2 (a) Cyclic voltammograms at PQQ-ADH/MWCNTs-modified GCE in 0.1 M acetate buffer solution (pH 5.5) containing $CaCl_2$ in the presence of 0.1 M ethanol at a scan rate of 10 mV s^{-1} under an argon atmosphere for various PQQ-ADH modification times; (b) illustration of DET between PQQ-ADH and the MWCNTs surface;[30,31,34,50] (c) catalytic oxidation current, PQQ-ADH surface concentration, PQQ-ADH layer number as a function of PQQ-ADH modification time.

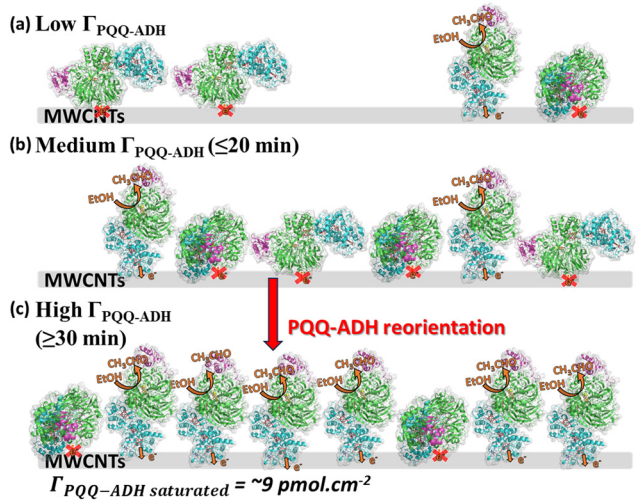

Fig. 3 Illustration of the suggested adsorption behavior for (a) low, (b) medium (≤20 min), and (c) higher (≥30 min) $\Gamma_{PQQ-ADH}$.

interactions may occur between each enzyme molecule with an increasing number of adsorbed PQQ-ADH molecules. Because PQQ-ADH is a membrane-binding enzyme, we predict that the hydrophobic surface of the enzyme molecules could interact with each other. Enzyme reorientation and softer surface rearrangement might occur from this interaction.[52] As a result, the hydrophobic interactions between each enzyme molecule are expected to increase with increasing enzyme surface concentration. This can be attributed to the sudden increase in the catalytic current at around 20–30 min of modification.

Sensitivity and selectivity of CNF film sensor

A CNF film sensor for detecting alcohol gas was fabricated as a three-electrode system, with PQQ-ADH/MWCNTs as the working electrode and PBI/MWCNTs as reference and counter electrodes on the CNF film. The observed CV at the CNF film sensor was the same as that obtained at the PQQ-ADH/MWCNTs/GCE (Fig. S18†). The reference electrode prepared using the PBI/MWCNTs exhibited high stability and repeatability in a laboratory environment (Fig. S19 and S20†). The CNF film sensor worked well despite being built with a thickness of 50 (± 5) μm and a compact design.

First, we investigated the ethanol gas sensitivity of the CNF film sensor using amperometry measurements at 0.2 V (*vs.* Ag|AgCl|saturated KCl) as the working electrode potential. The sensor exhibited an ultrahigh-sensitive response (Fig. S21†) compared to the previous electrochemical-based sensor.[21] The current response to the ethanol gas was obtained at a minimum concentration of 24 ppb. Further, the sensor exhibited a wide detection range up to 25 ppm. This sensor performance was sufficiently significant for detecting ethanol gas.[9,15,23,24,53] In addition, the sensitivity, detection range, and response time of our CNF film sensor were similar to those reported previously (Table 1). Furthermore, the sensor exhibited good repeatability. Within three time trials, the average deviation obtained was *ca.* 10 ± 5% at the ppb level and *ca.* 5 ± 2% at the ppm level (Fig. 4a). Additionally, the sensor exhibited an instant response within approximately 10 seconds after gaseous ethanol injection, which is important for skin gas monitoring.

Skin gas is a mixture of volatile organic compounds (VOCs), with acetone and alcohol being the most prevalent components.[9] To investigate the substrate selectivity of PQQ-ADH, CV measurements were carried out using a CNF film sensor for ethanol, methanol, 2-propanol acetone, and 1-propanol gases. Based on the CV results, the CNF film sensor exhibited a highly selective reaction with ethanol and 1-propanol (Fig. 4b). The selectivity results were in accordance with earlier studies using optical assay analysis.[39,54]

Component structure of CNF film sensor

Other materials have also been investigated for use as sensor film components. Tissue paper, baking paper, filter paper, plastic, and copy paper have been used for sensor-based film platforms (Fig. S22†). The analyses indicated that the CNF film sensor was lightweight, had sufficient water absorption capacity, and was suitable for maintaining appropriate moisture retention for electrochemistry (Table S1†). Additionally, an SEM image analysis of the CNF film sensor revealed that the outer layer of the CNF initially exhibited a smooth structure (Fig. 5a) with hydrophilic characteristics (Table S1†). After the MWCNTs modification, the surface of the MWCNTs/CNF film exhibited hydrophobicity (Table S2†) and a sponge-like structure, as shown in Fig. 5(b). The MWCNTs/CNF film component has a unique structure with a hydrophobic character on the outside and a hydrophilic character on the inside (Fig. 5c). This type of structural combination has the following advantages: (1) the inner CNF carpet-like structure provides sufficient porosity to control ethanol gas diffusion through the film, and (2) the ability to maintain the three-phase interface for PQQ-ADH. Three-phase interfaces are well-

Table 1 Non-invasive ethanol gas detection with enzyme-based sensor

Enzyme	Detection mechanism	Detection range	Response time	Location of detection	Delay time (compared to breath)	Sensor type	Ref.
NADH/ADH	Fluorescence	26 ppb–554 ppm	2 min	Ear canal	13 min	Concentration type	22
NADH/ADH	Fluorescence	25 ppb–128 ppm	2 min	Palm of hand	22 min	Concentration type	23
NADH/ADH	Fluorescence	1 ppb–3.1 ppm	6 min	Volar wrist	40 min	Concentration type	24
PQQ-ADH	Amperometric	24 ppb–25 ppm	Seconds	Volar wrist	—	Flux type	This work

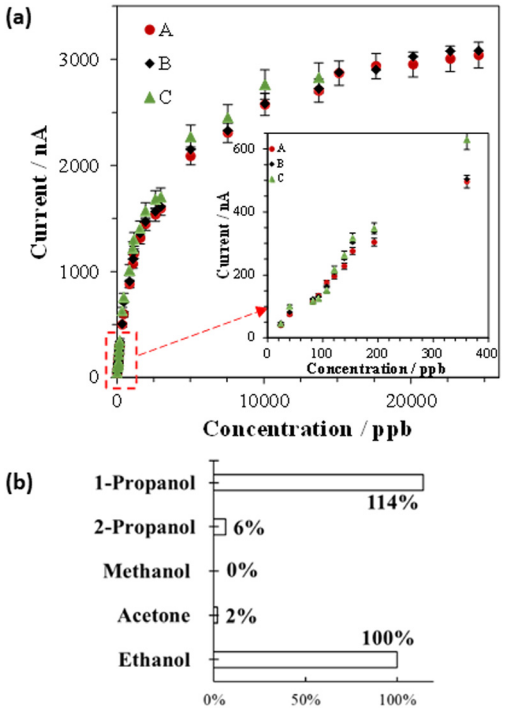

Fig. 4 (a) Sensitivity of CNF film sensor from triplicate amperometry measurements (marked as A–C). The insert zooms in parts for lower ethanol gas concentrations. (b) Selectivity of CNF film sensor as relative response compared to the ethanol gas.

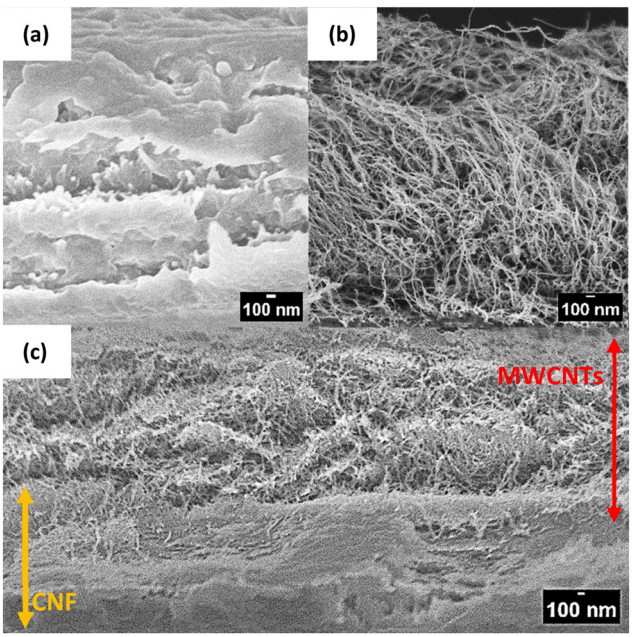

Fig. 5 SEM images of cross-sections of (a) CNF (b) MWCNTs working electrode, and (c) modified MWCNTs/CNF film.

known for achieving highly efficient reactions in the gas phase (Fig. S24†). The unique combination structure between MWCNTs and CNF may have yielded higher sensitivity than other film materials (Table S1†). Since cellulose is a biodegradable and environmentally friendly material,[29] it is expected that the CNF film sensor—a disposable sensor—will pose a minimal ecological footprint.

Non-invasive alcohol gas detection

The CNF film sensor was then used to monitor ethanol gas. The CNF film sensor was attached directly to a subject's left wrist, as shown in Fig. 6. The working electrode of the CNF film sensor was then applied at 0.2 V (*vs.* Ag|AgCl|saturated KCl). First, the baseline ethanol gas was measured for approximately ~16 min without alcohol consumption. The subject then drank 22.34 mL of 15% alcohol within a few seconds. Ethanol consumption was calculated as 40 mg per kg body weight, which is 10 times lower than the usual dose for alcohol tests.[15,22–24] After ethanol consumption, the ethanol gas concentration gradually increased and reached a peak approximately 3 minutes later (Fig. 7). This result was in line with the previous study,[15,55] where the smaller the alcohol dose consumed, the faster alcohol peak concentration was observed in BAC (blood alcohol concentration), TAC (transdermal alcohol concentration), and BrAC (breathe alcohol concentration). After reaching the peak, the alcohol flux signal gradually decreased towards baseline because of the detoxification process by liver,[15,56] which attributed to the decreases of BAC and measured alcohol gas. The CNF film sensor showed ultrahigh sensitivity, even under conditions of low ethanol consumption. The CNF film sensor is categorized as a flux-type sensor and showed a higher sensor rate constant *ca.* 10 times higher than the same flux-type sensor (Table S3†). The flux-type sensor output is proportional to the target molecule's permeability in the skin.[57] Thus, having an exceptionally sensitive sensor and high skin permeability allows faster response time. Moreover, metabolic conditions can be easily recognized through the declining slope of ethanol gas. After 4 hours of continuous operation, the CNF film sensor's surface lost its humidity and eventually dried.

We also conducted ethanol gas monitoring after consecutively higher doses of ethanol consumption (approximately 500 mg per kg body weight). A volunteer

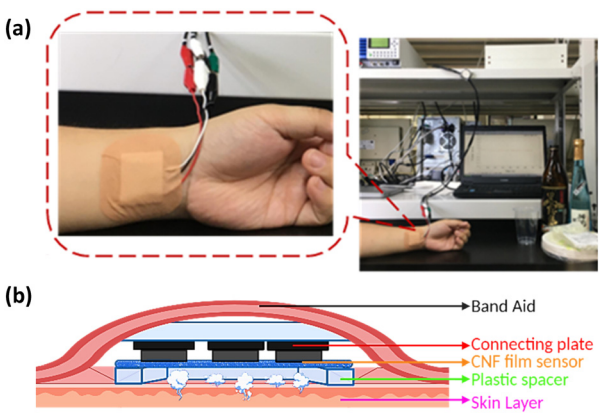

Fig. 6 (a) Photograph of non-invasive ethanol gas detection, and (b) illustration of a skin gas monitoring system.

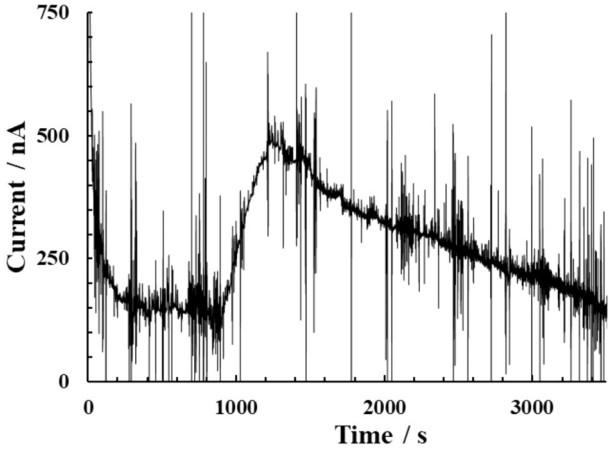

Fig. 7 Ethanol gas detection on a human subject using the cellulose nanofiber (CNF) film sensor under lower ethanol dose consumption after overnight (10 h) fasting.

continuously drank three types (5%, 12%, and 43%) of alcoholic beverages (under non-fasting conditions). The alcohol gas reached its first peak approximately 6 min after starting to drink 350 mL of beer (alcohol 5%) (Fig. S26†). The changes in alcohol flux signal highly depend on the liver processing alcohol and BAC.[15,56] Small spikes or noises observed in Fig. 7 and S26† were due to mechanical movement of the subject hand and feet (Fig. S27†). This monitoring of ethanol gas indicates that the prepared CNF film sensor is useful for the degree of intoxication as well as for monitoring the metabolic conditions in real-time.

Conclusions

In this study, we observed an interesting mismatch between the catalytic current based on DET with the MWCNTs surface and that with the PQQ-ADH surface concentrations. This interesting behavior could be attributed to the hydrophobic interactions between each PQQ-ADH molecule, which is a characteristic of a membrane-binding enzyme. The developed CNF film sensor exhibited ultrahigh sensitivity (~24 ppb) and specific ethanol detection with a wide detection range (~25 ppm). This ultra-high sensitivity could be because of the three-phase structured interface composed of MWCNTs, CNF, and PQQ-ADH. The CNF film sensor was successfully used to monitor ethanol gas continuously. To realize its practical use, the CNF film sensor's shelf-life needs to be thoroughly enhanced.

Data availability

The data supporting this article have been included as part of the ESI.† Further data is available upon reasonable request from the authors.

Author contributions

Citra Dewi Rakhmania: data curation, formal analysis, investigation, methodology, writing – original draft, visualization. Yosyi Izzudin Azhar: formal analysis, investigation, validation. Kenji Shida: performing SEM measurement, formal analysis, investigation, and validation. Erika Sinchi: perform permeator and GC measurement, formal analysis, investigation, and validation. Taiki Adachi, Keisei Sowa, Yuki Kitazumi, Osamu Shirai: resources, formal analysis, investigation, validation. Masato Tominaga: conceptualization, investigation, funding acquisition, writing – review & editing, supervision.

Conflicts of interest

There are no conflicts to declare.

Acknowledgements

MT acknowledges to Toshiaki Ogasawara Memorial Foundation for the Science and Technology Grants. This work was supported by the JST Adaptable and Seamless Technology Transfer Program through Target-driven R&D (A-STEP, MT, Grant No. JPMJTM205B). This work was the result of using research equipment shared in the MEXT Project for Promoting Public Utilization of Advanced Research Infrastructure (Program for Supporting the Introduction of the New Sharing System, Grant No. JPMXS0422400023).

References

1 M. Kurnik, E. Z. Pang and K. W. Plaxco, *Angew. Chem., Int. Ed.*, 2020, **59**, 18442–18445.
2 C. C. Mayorga-Martinez, R. Gusmão, Z. Sofer and M. Pumera, *Angew. Chem., Int. Ed.*, 2019, **58**, 134–138.
3 S. V. Somerville, Q. Li, J. Wordsworth, S. Jamali, M. R. Eskandarian, R. D. Tilley and J. J. Gooding, *Adv. Mater.*, 2024, **36**, e2211288.
4 F. L. R. Lucas, T. R. C. Piso, N. J. van der Heide, N. S. Galenkamp, J. Hermans, C. Wloka and G. Maglia, *Angew. Chem., Int. Ed.*, 2021, **60**, 22849–22855.
5 T. Arakawa, D. V. Dao and K. Mitsubayashi, *IEEJ Trans. Electr. Electron. Eng.*, 2022, **17**, 626–636.
6 H. C. Ates, P. Q. Nguyen, L. Gonzalez-Macia, E. Morales-Narváez, F. Güder, J. J. Collins and C. Dincer, *Nat. Rev. Mater.*, 2022, **7**, 887–907.
7 E. K. Lee, M. K. Kim and C. H. Lee, *Annu. Rev. Biomed. Eng.*, 2019, **21**, 299–323.
8 A. Annerino and P.-I. Gouma, *Sensors*, 2021, **21**, 7554.
9 T. Tsuda, T. Ohkuwa and H. Itoh, in *Gas Biology Research in Clinical Practice*, ed. T. Yoshikawa and Y. Naito, Karger, Basel, 2011, pp. 125–132.
10 L. Dormont, J. M. Bessière and A. Cohuet, *J. Chem. Ecol.*, 2013, **39**, 569–578.
11 A. Mitra, S. Choi, P. R. Boshier, A. Razumovskaya-Hough, I. Belluomo, P. Spanel and G. B. Hanna, *Metabolites*, 2022, **12**, 824.
12 K. Nose, T. Mizuno, N. Yamane, T. Kondo, H. Ohtani, S. Araki and T. Tsuda, *Anal. Sci.*, 2005, **21**, 1471–1474.
13 R. J. Dinis-Oliveira, *J. Clin. Med.*, 2021, **10**, 4637.

14 E. M. Hafez, M. A. Hamad, M. Fouad and A. Abdel-Lateff, *Hum. Exp. Toxicol.*, 2017, **36**, 445–450.
15 A. W. Jones, *WIREs Forensic Sci.*, 2019, **1**, e1340.
16 P. J. Perry, S. Doroudgar and P. Van Dyke, *J. Am. Acad. Psychiatry Law*, 2017, **45**, 429–438.
17 The United States MCIPAC Safety Office, **https://www.3rdmeb.marines.mil/Portals/110/Docs/Japan%20Driving.pdf?ver=WP7OFl3VKWNbn-VetspVLA%3D%3D**, (accessed 17/01/2024).
18 European Road Safety Observatory, **https://road-safety.transport.ec.europa.eu/system/files/2021-07/02-alcohol_en.pdf**, (accessed 17/01/2024).
19 The States Voice on Highway Safety, **https://www.ghsa.org/sites/default/files/2020-07/DrunkDrivingLaws_0720.pdf**, (accessed 17/01/2024).
20 World Health Organization, **https://cdn.who.int/media/docs/default-source/documents/health-topics/road-traffic-injuries/ifrc-drink-driving-2022-final.pdf?sfvrsn=f3e09010_6&download=true**, (accessed 17/01/2024).
21 B. Lansdorp, W. Ramsay, R. Hamidand and E. Strenk, *Sensors*, 2019, **19**, 2380.
22 K. Toma, S. Suzuki, T. Arakawa, Y. Iwasaki and K. Mitsubayashi, *Sci. Rep.*, 2021, **11**, 10415.
23 T. Arakawa, T. Suzuki, M. Tsujii, K. Iitani, P. J. Chien, M. Ye, K. Toma, Y. Iwasaki and K. Mitsubayashi, *Biosens. Bioelectron.*, 2019, **129**, 245–253.
24 T. Arakawa, T. Aota, K. Iitani, K. Toma, Y. Iwasaki and K. Mitsubayashi, *Talanta*, 2020, **219**, 121187.
25 T. Arakawa, K. Kita, X. Wang, K. Miyajima, K. Toma and K. Mitsubayashi, *Biosens. Bioelectron.*, 2015, **67**, 570–575.
26 B. Lawson, K. Aguir, T. Fiorido, V. Martini-Laithier, R. Bouchakour and S. Burtey, *Sens. Actuators, B*, 2019, **280**, 306–312.
27 F. E. Annanouch, V. Martini, T. Fiorido, B. Lawson, K. Aguir and M. Bendahan, *Sensors*, 2021, **21**, 6852.
28 J. Kim, I. Jeerapan, J. R. Sempionatto, A. Barfidokht, R. K. Mishra, A. S. Campbell, L. J. Hubble and J. Wang, *Acc. Chem. Res.*, 2018, **51**, 2820–2828.
29 R. Motohashi and I. Hanasaki, *Nanoscale Adv.*, 2019, **1**, 421–429.
30 T. Adachi, K. Sowa, Y. Kitazumi, O. Shirai and K. Kano, *Bioelectrochemistry*, 2022, **143**, 107992.
31 T. Adachi, T. Miyata, F. Makino, H. Tanaka, K. Namba, K. Kano, K. Sowa, Y. Kitazumi and O. Shirai, *ACS Catal.*, 2023, **13**, 7955–7965.
32 S. R. Sari, M. Tsushida, T. Sato and M. Tominaga, *Mater. Adv.*, 2022, **3**, 2018–2025.
33 S. R. Sari, E. Sinchi, K. Shida, Y. Kusumawati, K. A. Madurani, F. Kurniawan and M. Tominaga, *Analyst*, 2023, **148**, 2932–2940.
34 P. Kanninen, V. Ruiz, T. Kallio, I. V. Anoshkin, E. I. Kauppinen and K. Kontturi, *Electrochem. Commun.*, 2010, **12**, 1257–1260.
35 T. Kondo, R. Kose, H. Naito and W. Kasai, *Carbohydr. Polym.*, 2014, **112**, 284–290.
36 S. Yokota, K. Kamada, A. Sugiyama and T. Kondo, *Carbohydr. Polym.*, 2019, **226**, 115293.
37 H. Zhang, L. Shi, J. Lin, M. Sun and D. Wei, *Biotechnol. Lett.*, 2016, **38**, 1131–1138.
38 C. Prust, M. Hoffmeister, H. Liesegang, A. Wiezer, W. F. Fricke, A. Ehrenreich, G. Gottschalk and U. Deppenmeier, *Nat. Biotechnol.*, 2005, **23**, 195–200.
39 O. Adachi, K. Tayama, E. Shinagawa, K. Matsushita and M. Ameyama, *Agric. Biol. Chem.*, 1978, **42**, 2045–2056.
40 M. Tominaga, K. Kuwahara, M. Tsushida and K. Shida, *RSC Adv.*, 2020, **10**, 22120–22125.
41 J. K. Park, H. J. Yee and S. T. Kim, *Biosens. Bioelectron.*, 1995, **10**, 587–594.
42 J. K. Park, H. J. Yee, K. S. Lee, W. Y. Lee, M. C. Shin, T. H. Kim and S. R. Kim, *Anal. Chim. Acta*, 1999, **390**, 83–91.
43 M. Tominaga, N. Hirata and I. Taniguchi, *Electrochem. Commun.*, 2005, **7**, 1423–1428.
44 M. Tominaga, K. Soejima, M. Matsumoto and I. Taniguchi, *J. Electroanal. Chem.*, 2005, **579**, 51–58.
45 G. Davis, H. A. O. Hill, W. J. Aston, I. J. Higgins and A. P. F. Turner, *Enzyme Microb. Technol.*, 1983, **5**, 383–388.
46 T. Ikeda, D. Kobayashi, F. Matsushita, T. Sagara and K. Niki, *J. Electroanal. Chem.*, 1993, **361**, 221–228.
47 B. L. Treu, R. Arechederra and S. D. Minteer, *J. Nanosci. Nanotechnol.*, 2009, **9**, 2374–2380.
48 S. A. Neto, D. P. Hickey, R. D. Milton, A. R. De Andrade and S. D. Minteer, *Biosens. Bioelectron.*, 2015, **72**, 247–254.
49 M. Tominaga, M. Togami, M. Tsushida and D. Kawai, *Anal. Chem.*, 2014, **86**, 5053–5060.
50 C. Anthony, *Biochem. J.*, 1996, **320**, 697–771.
51 S. A. Neto, T. S. Almeida, D. M. Belnap, S. D. Minteer and A. R. De Andrade, *J. Power Sources*, 2015, **273**, 1065–1072.
52 M. F. Mora, C. E. Giacomelli and C. D. Garcia, *Anal. Chem.*, 2009, **81**, 1016–1022.
53 F. M. Schmidt, O. Vaittinen, M. Metsälä, M. Lehto, C. Forsblom, P. H. Groop and L. Halonen, *J. Breath Res.*, 2013, **7**, 017109.
54 O. Adachi, E. Miyagawa, E. Shinagawa, K. Matsushita and M. Ameyama, *Agric. Biol. Chem.*, 1978, **42**, 2331–2340.
55 T. E. Karns-Wright, J. D. Roache, N. Hill-Kapturczak, Y. Liang, J. Mullen and D. M. Dougherty, *Alcohol Alcohol.*, 2017, **52**, 35–41.
56 J. C. Anderson and M. P. Hlastala, *J. Appl. Physiol.*, 2006, **100**, 649–655.
57 B. M. Lansdorp, *Bisensors*, 2023, **13**, 845.